CHALMERS
UNIVERSITY OF TECHNOLOGY

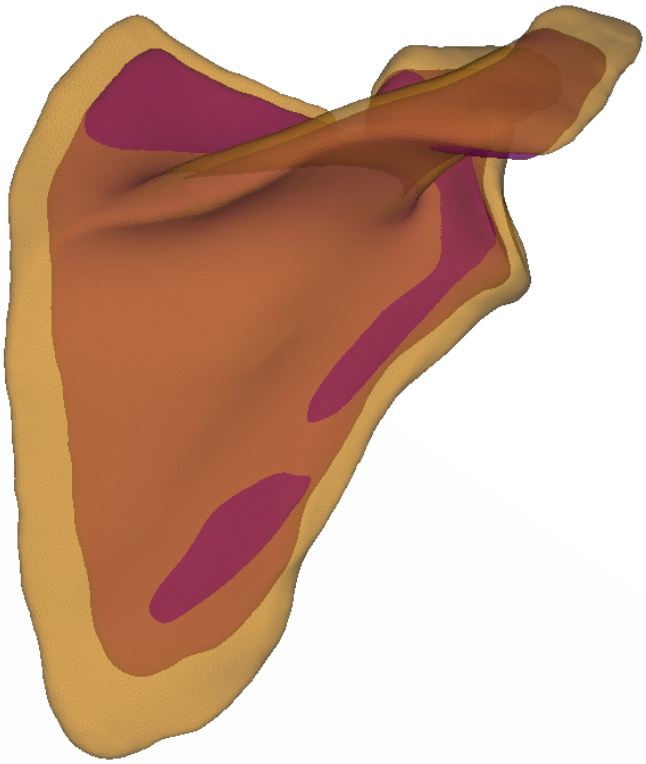

Development of a statistical shape model of the human scapula

Development of a statistical shape model of the human scapula for improvement in vehicle safety aspects

Master's thesis in Biomedical Engineering and Complex Adaptive Systems

SEYED AMIRMOHAMMAD ABOTORABI
FILIP AHLMAN

DEPARTMENT OF MECHANICS AND MARITIME SCIENCES
CHALMERS UNIVERSITY OF TECHNOLOGY
Gothenburg, Sweden 2025
www.chalmers.se

Master's thesis in Biomedical Engineering and Complex Adaptive Systems 2025

Development of a statistical shape model of the human scapula

Development of a statistical shape model of the human scapula for improvement in vehicle safety aspects

Seyed Amirmohammad Abotorabi
Filip Ahlman

CHALMERS
UNIVERSITY OF TECHNOLOGY

Department of Mechanics and Maritime Sciences
Division of Vehicle Safety
Chalmers University of Technology
Gothenburg, Sweden 2025

Development of a statistical shape model of the human scapula
for improvement in vehicle safety aspects
Seyed Amirmohammad Abotorabi
Filip Ahlman

Supervisor: Johan Iraeus, Chiara Rosanna Fichera, Department of Mechanics and Maritime Sciences
Examiner: Johan Davidsson, Department of Mechanics and Maritime Sciences

Master's Thesis 2025
Department of Mechanics and Maritime Sciences
Division of Vehicle Safety
Chalmers University of Technology
SE-412 96 Gothenburg
Telephone +46 31 772 1000

Typeset in LaTeX
Printed by Chalmers Reproservice
Gothenburg, Sweden 2025

Development of a statistical shape model of the human scapula
for improvement in vehicle safety aspects
Seyed Amirmohammad Abotorabi
Filip Ahlman
Department of Mechanics and Maritime Sciences
Division of Vehicle Safety
Chalmers University of Technology

Abstract

The human scapula is the fundamental structure of the shoulder and an anatomical landmark for upper limb movements. Understanding variations in scapula shape can influence biomechanical modeling, clinical diagnosis, and safety simulation, particularly in vehicle crash testing. The aim of this study is to develop a Statistical Shape Model (SSM) of the human scapula bone from computed tomography (CT) image data segmentations to analyze and describe the variability in the population based on sex, height, age, and BMI.

A dataset comprising 70 segmented scapulae derived from an original set of 230 segmented scapulae, including healthy samples and samples with Hill-Sachs lesions, some of which are considered unhealthy, was used for this study. The landmarking set-up consisted of 45 landmarks in total, including 20 anatomical landmarks and 25 pseudo-landmarks placed along splines, which provide reliable reference points for shape analysis. Morphing techniques, performed primarily in Python code, were used to standardize the mesh structures of scapulae by mapping every sample onto a common average model. For ease of comparison, General Procrustes Analysis (GPA) was used first to remove position, orientation, and scale variance, and then Principal Component Analysis (PCA) to capture the main modes of shape variation in the dataset. Then, a regression model is used on the principal components of the PCA to study variations based on population data.

The resulting SSM provides valuable information on the variation of the anatomical scapula of the population and how demographic factors influence bone shape and size. The results have potential applications to personalized biomechanical modeling, clinical diagnostics, and improved occupant protection in vehicle crash simulations.

Keywords: Human body model, statistical shape model, scapula, general procrustes analysis, principal component analysis, Hills-Sachs lesion.

Preface

This report presents the outcome of our master's thesis project carried out at the Department of Mechanics and Maritime Sciences at Chalmers University of Technology during the spring of 2025.

Acknowledgements

First of all, we would like to thank our supervisors, Chiara and Johan, for their help; from theory to writing, we received weekly support, and we are truly grateful. Thanks to Autoliv for having an interest in and supporting our project and others like it. Finally, thanks to our family and our friends for their endless support.

Amir and Filip, Gothenburg, June 2025

List of Acronyms

Below is the list of acronyms that have been used throughout this thesis listed in alphabetical order:

BMI	Body Mass Index
CT	Computed Tomography
GPA	General Procrustes Analysis
HBM	Human Body Models
MRI	Magnetic Resonance Imaging
PCA	Principal Component Analysis
PC	Principal Component
SSM	Statistical Shape Model
SVD	Singular Value Decomposition

Contents

List of Figures

List of Tables

1
Introduction

Magnetic Resonance Imaging (MRI), Computed Tomography (CT), and ultrasonic imaging are some of the medical imaging techniques that are used to get detailed 3D images of the interior of the human body. In many cases, these images are used for diagnostics. In other cases, these images are used as input to build models, like digital twins. In other cases, for example, in archaeology or forensic sciences, many images of various subjects are assembled, and statistical models are developed that describe the variation among populations to be able to conclude what is normal and to be able to estimate height, sex, and age from a single bone [1].

1.1 The scapula

The shoulder blade, or scapula, is a flat, broad, triangular bone that makes up part of the shoulder girdle. It connects the humerus to the clavicle and, along with the head of the humerus, makes up the glenohumeral joint through its connection to the glenohumeral cavity. The scapula also provides important attachment points for several groups of muscles that help move and stabilize the shoulder [2].

The scapula is fixated to the axial skeleton solely via the clavicle. Motions of the shoulder blade mostly facilitate the movements of the upper arm. In some parts of the supraspinous and infraspinous fossa, the thickness of the cortical bone is less than 1 millimeter and looks semitranslucent when observed against the light [3].

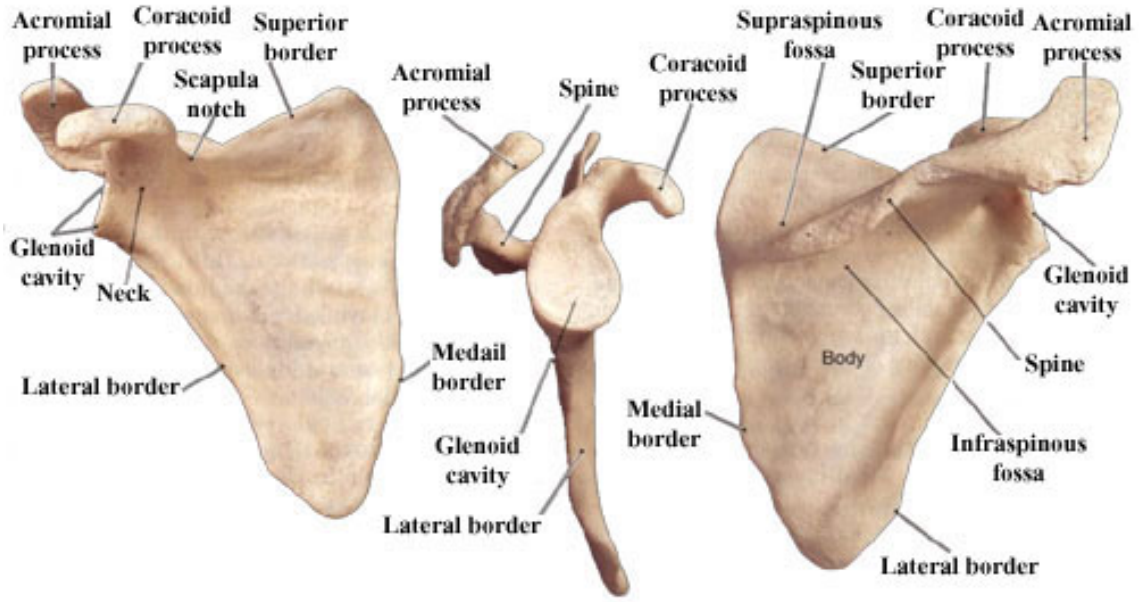

Figure 1.1: Scapula features. Image adapted from [4].

1.2 The epidemiology of scapular fractures

Scapular fractures are relatively rare, accounting for less than 1% of all fractures and around 3-5% of shoulder girdle fractures. A comprehensive study by Schmidt. et al. in Sweden analyzed 3,930 patients with 3,973 scapular fractures. The mean age was 58 years, with 64% being men [5]. High energy trauma caused 22% of these fractures and 21% had at least one associated fracture. Glenoid neck and scapular body fractures were often due to high-energy injuries, while falls of the same level commonly cause glenoid rim and intraarticular glenoid fractures [5]. The study reported an annual incidence of 10 per 100,000 inhabitants, with 30% of fractures involving the glenoid cavity. The mean age at fracture was significantly higher in women than in men, at 64 years compared to 49 years [6].

Epidemiological studies on scapular fractures by Ideberg R. et al and Tuček M. et al show that with increasing age, women are more frequently affected than men, and low-energy mechanisms are more common, probably due to osteoporosis [7][8]. Osteoporosis is a bone disease characterized by the reduction of bone mineral density or bone mass, or the alteration in the structure and strength of the bone. It ultimately causes bones to become weaker, thereby increasing the risk of fractures [9].

Hill-Sachs lesion is an anterior dislocation or instability of the glenohumeral joint with a bony defect or "dent" of the postero-supero-lateral humeral head [10][11]. It usually occurs in association with a Bankart lesion of the glenoid [12].

1.3 Statistical Shape Models and Human Body Models

Statistical Shape Models (SSMs) are geometric models for describing a collection of semantically consistent objects in space-efficient form, representing the mean shape and shape variation over large numbers of three-dimensional objects. Building an SSM entails specifying correspondence mapping between shapes, typically accomplished through parameterization to enable mathematical investigation of the variation of shape. In addition to shape, appearance features—i.e., color or intensity from imaging modalities like CT or MRI can also be used to combine them and produce Statistical Shape and Appearance Models (SSAMs). SSMs have been applied to human organs, bony structures, faces, and bodies, with clinical applications for cohort anatomical data analysis and correlation of typical shapes with demographic or epidemiologic measures. Large SSM datasets using statistical or machine learning methods permit characteristic clusters and advanced diagnostic disease scoring to be determined [13].

SSMs, also known as morphometric models, are used to study anatomical variations. The Vehicle Safety Division at the Department of Mechanical and Maritime Sciences at Chalmers University of Technology has been developing finite element models of the Human Body Model (HBM) to develop human surrogates for the simulation of a vehicle crash, with the final goal of improving safety and saving lives. These HBMs apply SSMs to represent different segments of the population and accurately capture population variation. The goal is to improve the accuracy and relevance of crash simulators covering the whole population at risk [14].

HBMs are also critical resources for researching occupant safety in some areas, such as autonomous vehicles (AV), because they allow an analysis of a larger set of occupant positions and crash scenarios compared to traditional experimental dummies [15]. Using HBMs, the crash analysis simulations can be done for many occupants and other road users [16].

1.4 Aim & Objectives

The study aims to develop a SSM of the human scapula bone from data segmentations.

The objective is to analyze and describe the variability in the population based on sex, height, age, and BMI to see the differences in the shape of the scapula bone.

1.5 Ethical Considerations

The SSM developed in this thesis is primarily geared towards reducing the risk of body injury through improved comprehension of anatomical variation. This information can be translated into clinical application by helping the diagnosis of scapular fractures, treatment planning, and management, ultimately resulting in safer and more effective patient treatment [17].

However, one should consider potential unintended uses of these shapes and finite element models, such as experimentation with ammunition for weapons. These uses would be specifically counter to the ethical intent and primary objective of this research, and that objective is solely directed at enhancing medical and vehicle safety.

All data used within this project are anonymized for confidentiality and privacy purposes, and it is not possible to identify individual data of research participants from the models. In addition, the SSM represents the typical anatomical variations present in the majority of the population. Thus, it may not represent outliers caused by pathological conditions, developmental deformations, or unusual anatomical states.

1.6 Limitations

There were several limitations in the development of the SSM in this thesis. One was that although the data set used was relatively large, it would not necessarily include all the variability of the larger population. The samples taken were both healthy scapulae and those with Hill-Sachs lesions, but other diseases or unusual deformities are probably not well represented, and therefore may limit the model to being effectiveness for the full range of clinical cases.

In addition, the geometries used for analysis were pre-segmented before the current research. So, there is no control over the accuracy of the samples, which could influence the quality and reliability of the models created.

Furthermore, the samples were from a specific subpopulation, as mentioned in the Method and the Dataset sections. It is not necessarily generalizable to other ethnic groups or populations, and therefore could restrict the findings from being applied to larger populations.

Finally, there are certain other potentially covariate-influential variables, such as medical condition, exercise, or work activity, that will not have been accounted for in the current analysis. By removing these variables, potentially influential factors that could have an effect on the variation of scapular shape could be missed. Several of these limitations, e.g., removing other covariates, were a product of time constraints within the project schedule.

2
Theory

2.1 Singular value decomposition

For a real $m \times n$ matrix M, the SVD of M is defined as:

$$M = U\Sigma V^T, \tag{2.1}$$

where U is an orthogonal $m \times m$ matrix with left singular column vectors of M. Σ is a $m \times n$ diagonal matrix with the singular values of M in descending order. V^T is the transpose of V, which is a $n \times n$ matrix with columns as right singular vectors of M.

2.2 Kabsch's algorithm for optimal rotation matrix using singular value decomposition

Let P and Q be two sets containing N points in $\mathbb{R}^n$ [18]. The optimal rotation matrix R which minimizes $\sum_{k=1}^{N} |R_{q_k - p_k}|$ where q_k, p_k are rows in P and Q, then R can be calculated by:

$$\begin{aligned} H &:= P^T Q, \\ H &= U\Sigma V^T, \\ d &= det(U)det(V), \\ R &= U \begin{pmatrix} 1 & 0 & 0 \\ 0 & 1 & 0 \\ 0 & 0 & d \end{pmatrix} V^T. \end{aligned} \tag{2.2}$$

Where $U\Sigma V^T$ is the singular value decomposition of H.

2.3 Principal component analysis using singular value decomposition

Let X be a $m \times n$ matrix with n samples and m variables. From the singular value decomposition of X we get:

$$X = U\Sigma V^T, \tag{2.3}$$

where V are the principal components of X and $U\Sigma$ are the scores of X [19].

2.4 Multivariate linear regression with the ordinary least squares method

The multivariate linear regression takes the form,

$$\begin{aligned} y_1 &= \beta_0 + \beta_1 x_1 1 + ... \beta_n x_n 1 + \epsilon_1, \\ y_2 &= \beta_0 + \beta_1 x_1 2 + ... \beta_n x_n 2 + \epsilon_2, \\ &\vdots \\ y_n &= \beta_0 + \beta_1 x_n 1 + ... \beta_n x_n n + \epsilon_n \end{aligned} \tag{2.4}$$

where $x_1, x_2, ..., x_n$ are the variables, $\beta_0, \beta_1, ..., \beta_n$ are constants, and ϵ_n is the error. This problem can be solved by using a least squares estimator where we minimize ϵ^2. Equation 2.4 can also be written as:

$$\epsilon = X\beta - y, \tag{2.5}$$

where $\epsilon = [\epsilon_1, \epsilon_2, ...\epsilon_n]$, $\beta = [\beta_0, \beta_1, ..., \beta_n]$, $y = [y_1, y_2, ...y_n]$, and $X = \begin{pmatrix} 1 & x_{11} & ... & x_{1k} \\ 1 & x_{21} & ... & ... \\ ... & ... & ... & ... \\ 1 & x_{n1} & ... & x_{nk} \end{pmatrix}$.

Solving for $min(\epsilon^2)$ given the variables β [20],

$$\begin{aligned} \epsilon^2 = \epsilon^T \epsilon &= (y - X\beta)^T (y - X\beta), \\ min(\epsilon^2)|_\beta &= yy^T - 2\beta^T X^T y + X^T X\beta, \\ \frac{\partial(\epsilon^2)}{\partial(\beta)} &= -2X^T y + 2X^T Xb = 0, \\ X^T X\beta &= X^T y, \\ \beta &= (X^T X)^{-1}(X^T y). \end{aligned} \tag{2.6}$$

3
Method

Several steps are needed to create a SSM for the scapula. The segmented meshes were used from the CT images to isolate the scapula bones. Landmarks need to be applied to the segmented meshes to capture shape details. Each set of landmarks is used to morph a source mesh into the shape of those landmarks. These morphed meshes are then aligned through General Procrustes Analysis (GPA). The aligned points are then combined into a single set of data, to which Principal Component Analysis (PCA) is applied. From the PCA, principal component (PC) scores provide a target for the model, and the effect of each component serves as a tool to analyze it. A regression model is then formed where the input is the sex, age, height, and BMI of a sample scapula, and the output is the PC scores from the corresponding scapula. The regression model can then be used to predict a new scapula based on the same inputs.

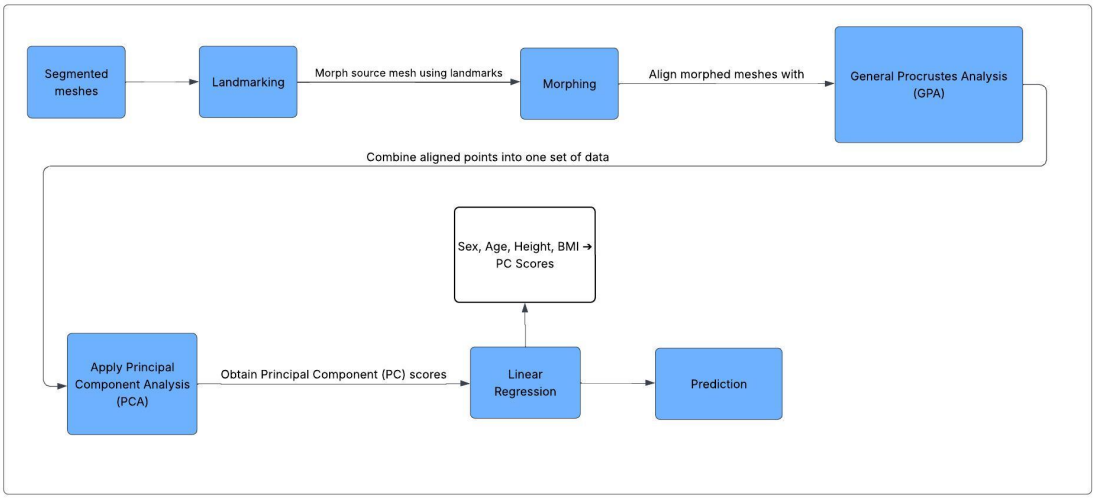

Figure 3.1: Flowchart connecting the parts described in the following sections

3.1 Dataset

The data used is "3D models of the human scapula and humerus with defined anatomic landmarks" [21], an open-source data set of segmented scapulae. This dataset comprises 230 segmented scapulae, including both healthy samples and those with Hill-Sachs lesions. The five defined anatomical landmarks included in

the dataset were not used. The reason we did not use the included anatomical landmarks is that we cannot ascertain the quality of the landmarks when we do not possess the required anatomical knowledge to validate them.

The dataset, which we knew from the start was too large to landmark within the time we had. A smaller set with higher quality and with a more even distribution of variables would be preferable for the regression model. The first filter was one column in the data named "note" where there were written about potential issues with the segmentation or other irregularities were written. We decided that every scapula with a note would be removed from our data. The dataset had a higher concentration of people in the age bracket 40-60 years old, and some were removed to get closer to a uniform distribution.

After filtering the dataset based on demographics and if there were any issues with the segmentation, there were 130 samples left. However, due to the limited time, the total number of landmarked scapulae was 70, 33 of which had different levels of Hill-Sachs lesions.

3.2 The demographic distribution after filtering

The demographic distribution is shown in Table: 3.1.

	Mean	SD
Age	44.6 (years)	18.9 (years)
BMI	25.6 ($\frac{kg}{m^2}$)	5.11 ($\frac{kg}{m^2}$)
Height	1.74(m)	0.11(m)

Table 3.1: The mean and standard deviation for age, BMI, and height for the data used as samples.

The charts in Figure: 3.2 show the sex, height, age, and BMI distribution of the 70 samples used.

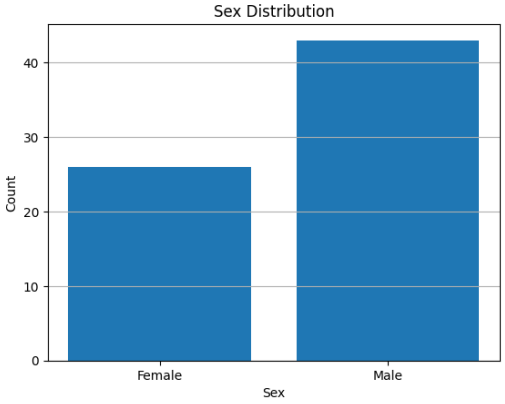

(a) Sex distribution

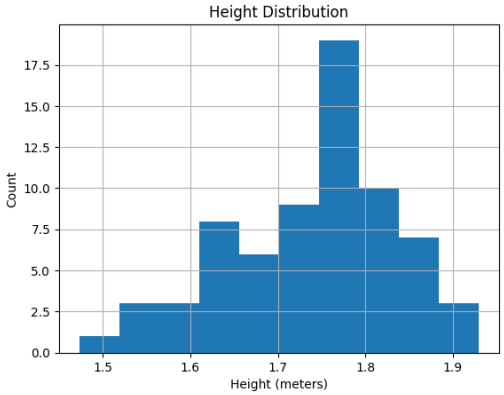

(b) Height distribution

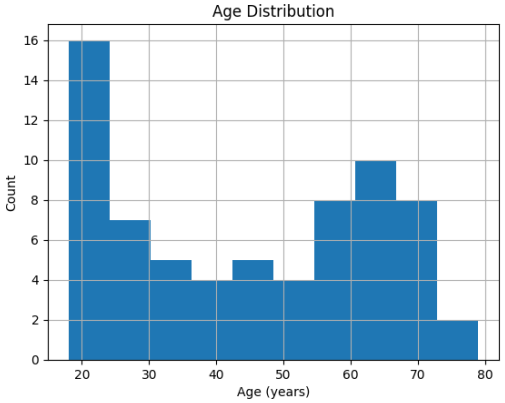

(c) Age distribution

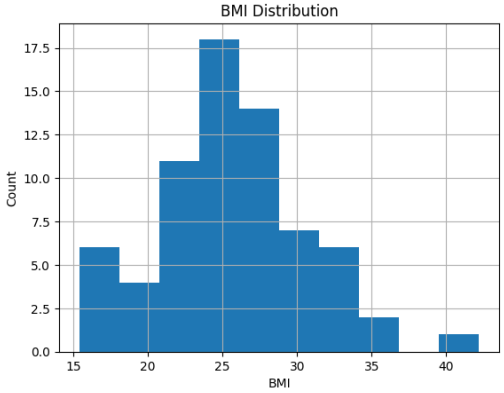

(d) BMI distribution

Figure 3.2: Distribution histogram of the dataset: (a) Sex, (b) Height, (c) Age, and (d) BMI

3.3 Landmarking

Landmarking is the process of placing a set of points onto an object to highlight some feature. A landmark in itself is just a position in space; in a three-dimensional space, it would just be the x, y, and z coordinates. The placement and design of the set of landmarks are affected by how rigid and consistent the rules are for placement. The placement could be the anatomical connection of a musculature to a bone, the connection to another bone, or more vaguely, the midpoint of a curve. Creating a set of landmarks is striking a balance between the amount of landmark density needed for one's purpose and the amount of time landmarking will take. The ideal landmark is consistent in location and has a high rate of information yield.

Our purpose for landmarking is twofold: Firstly, for the morph to be closer to the target sample. Secondly, the calculation for the rotational matrix in the GPA.

Figure 3.3 shows the landmark design used in this project for the scapula, consist-

ing of 45 landmarks in total, including 20 anatomical landmarks and 25 pseudo-landmarks generated from splines of equidistant positions between anatomical landmarks. The 3D-slicer is used in this method. For further details, the explanation of each landmark used is presented in Table: A.1.

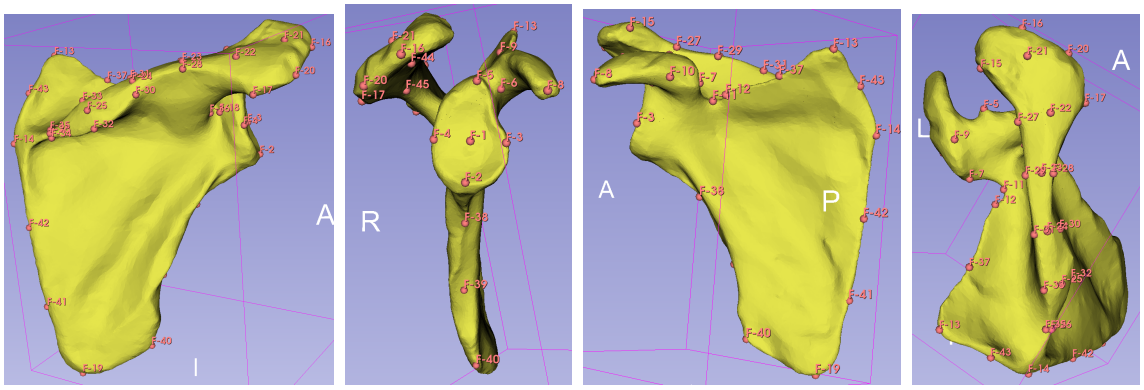

Figure 3.3: Visualization of the 45 landmarks used for shape analysis, shown on four different views of the scapula. Each landmark is indicated with a red label and placed at specific anatomical or pseudo-anatomical positions on the scapular surface.

3.4 Morphing

The goal of morphing is to create a replica of a target mesh through a source mesh, using landmarks and interpolation. The success of a morph hinges on the quality and quantity of the landmarks used in the morphing as well as the quality of the source mesh. The target mesh and the morphed source mesh will be identical on each landmark, and interpolation is only done between landmarks.

We used Python and, specifically, the 'morphing' function from the infepy GitHub repository [22]. Morphing requires a target mesh, a source mesh, and a set of landmarks for each mesh. The morphing function gives the output of an interpolated version of the target mesh with the source as a base. We refer to this interpolated source as a "morph".

A source mesh is chosen as a representative of the larger sample. This source should be as average as possible in variations, with no deviations or curves within the bone. After selecting a good source mesh, which belongs to a 24-year-old male, smoothing of this mesh can be done to remove unwanted smaller variations and surface noise.

The source used is shown in Figure: 3.4, selected for its generally featureless appearance and lack of deformations. The source was smoothed in ANSA using the "Noise" function to slightly reduce its size and remove smaller blemishes on the surface.

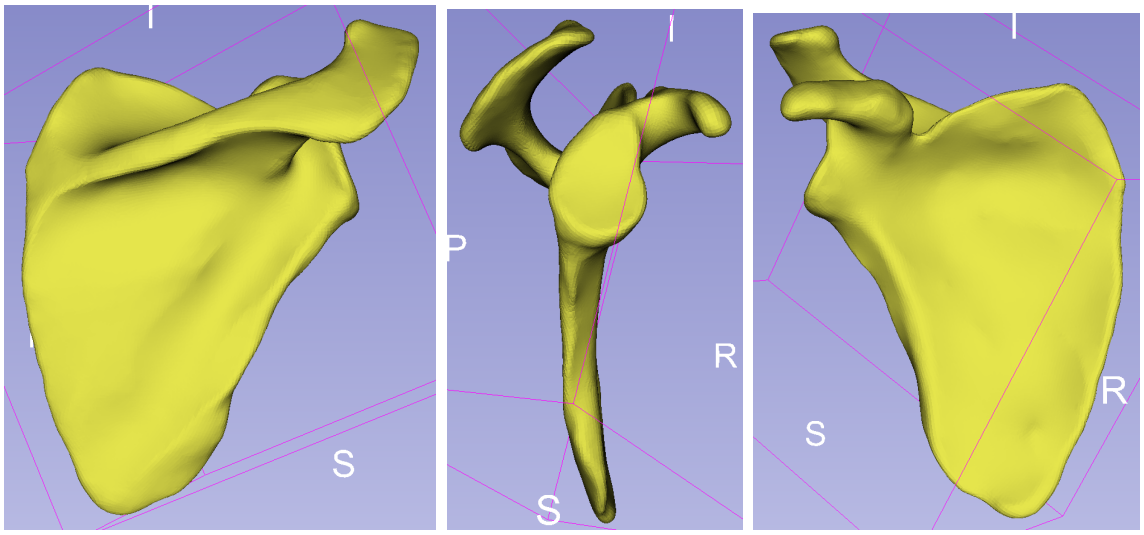

Figure 3.4: The scapula sample used as the source, after smoothing. This scapula is in the healthy dataset, belongs to a 24-year-old male.

3.5 General Procrustes analysis

Since the created morphs generally are not guaranteed to be in the same place in space, some alignment is necessary. GPA seeks to remedy this through three parameters, the first being a mean value calculation that aligns the centers of each mesh with each other. The second is a scale factor, aligning with the sheer size of the object. The third is a rotation, calculated through a rotational matrix through kabsch algorithm in equation: 2.2. After applying a center adjustment, scaling the object up or down, and rotating the object optimally, all morphed scapulae will be aligned in space.

The scale of each scapula can be included either through the GPA parameter or in (usually) the first component of the PCA. We did not use any scaling parameter for the GPA and instead included the effect of scale inside the principal components; this is merely a choice in interpretation and does not affect the outcome.

3.6 Principal component analysis

The scapulae have now been morphed and aligned, giving us a vast set of data points to analyze differences. By applying PCA to our data, we can observe differences in the entirety of the scapula instead of splitting the data up into sections and analyzing it part by part. PCA has the benefit of explaining a lot through dimensionality reduction, but does limit the understanding we have over how the resulting data behaves. Following the theory from 2.3, applying PCA to our set of scapulae, the output will be a set of scores called PC scores. We can modify the scores for each principal component directly to get a better understanding of what effect that component has on the anatomy of the scapula.

3.7 Linear regression

The linear regression model starts with a selection of demographics from the dataset: sex, age, height, and BMI. In addition to the previously stated variables, we also added the variable $sex * height$ as a control for the possible covariance between sex and height. We want to create a regression model that links these variables into a mesh; the regression model could then be used to predict a scapula based on the input demographics. One approach is to make a model between these variables and the PC scores. If the PC-scores can be predicted from a set of variables, then the inverse transformation from PCA can be applied to the scores, and a mesh can be created. One regression model is created for each principal component and is used to generate one score. The problem is now in the same form as the multivariate linear regression example in 2.6 and can be solved with ordinary least squares. The variables in every regression model are checked for significance and then remodeled with only the significant variables.

4

Results

This section presents the results of the data filtering, landmarking, morphing, each principal component, and the regression.

4.1 Morphing

In Figure: 4.1, the results of a morph compared to a sample scapula we are trying to replicate through morphing, the goal here is to as closely as possible overlap these meshes. By the design of our set-up, we have more landmarks at the top part of the scapula, which is more complex. For example, around the spine of the scapula, we have a very high density of landmarks, which results in a good approximation for the resulting morph. Some edges of the border have a worse overlap from not have the density of landmarks required to cover the entire border. The thickness between the infraspinatus fossa and the subscapular fossa does not have any landmarks, and the resulting morph is only interpolated in these locations.

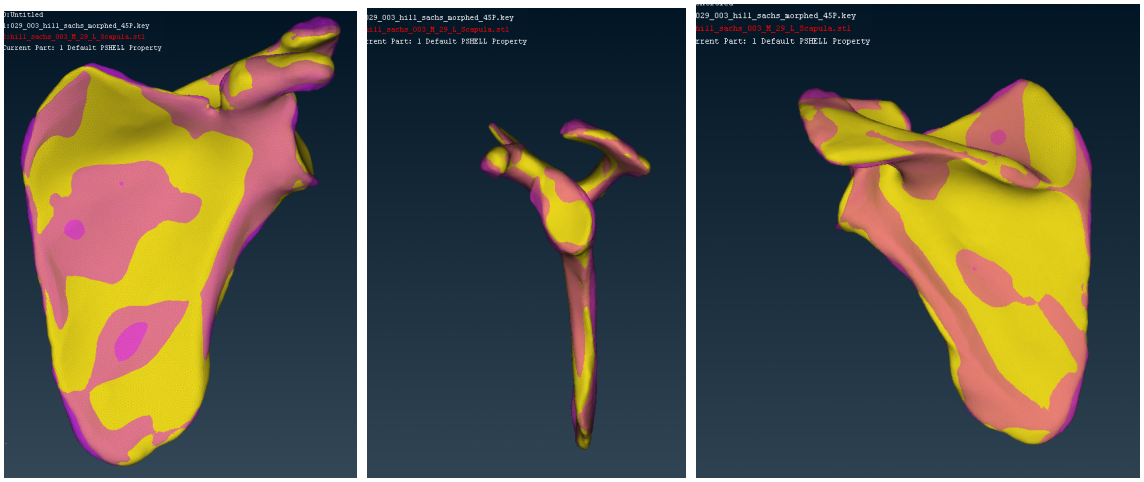

Figure 4.1: The resulting morph of sample 03 from the Hill-Sachs dataset compared to the actual sample 03. The yellow scapula belongs to the morphed mesh, and purple is the sample 03.

4.2 Explained variance

Figure 4.2 shows the cumulative explained variance for the principal components. The first component already explains close to 60% and we are close to 90% at component 10. The highest number of components used was set at below 95% of the cumulative variance explained by the principal components, resulting in 16 components.

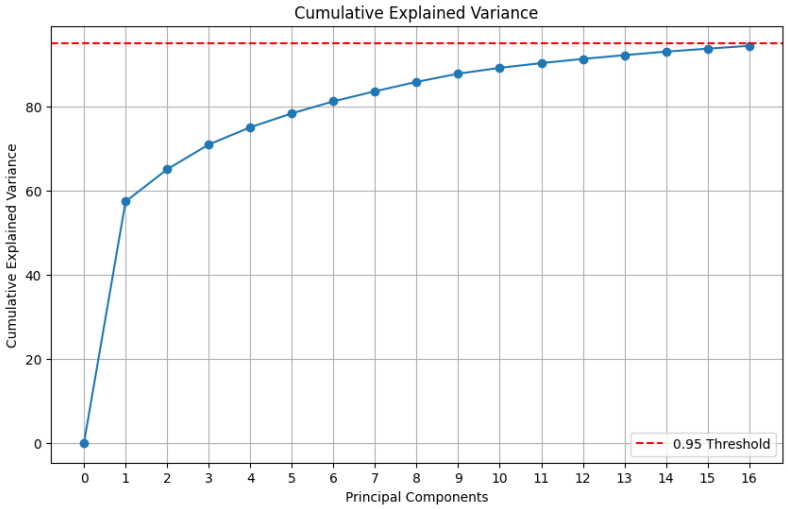

Figure 4.2: Cumulative explained variance for the principal components and 95% marked in dashed red.

4.3 The effect of the principal components on the model

Figures 4.3 - 4.7 show the effect that each principal component would have on the model, given that it is used. Principal components are visualized here by modifying the source mesh (μ) through one standard deviation of the principal component scores (σ).
In Figure 4.3, component 1 contains most of the scale that we expect to see from the difference in height and sex. The largest difference is between the superior and inferior angles, while a smaller difference can be seen in the size of the glenoid fossa.

In Figure 4.4, a curvature difference can be spotted for the entirety of the scapula, with yellow being more curved while purple is less curved.
In Figure 4.5, purple is wider close to the inferior and superior angles, while yellow is a bit narrower.
In Figure 4.6, a curvature of the entire scapula can be seen, purple being more straight and yellow slightly bent.
In Figure 4.7, the largest difference can be seen on the glenoid fossa and down the lateral border. A smaller difference between the superior and inferior angles can

also be seen.

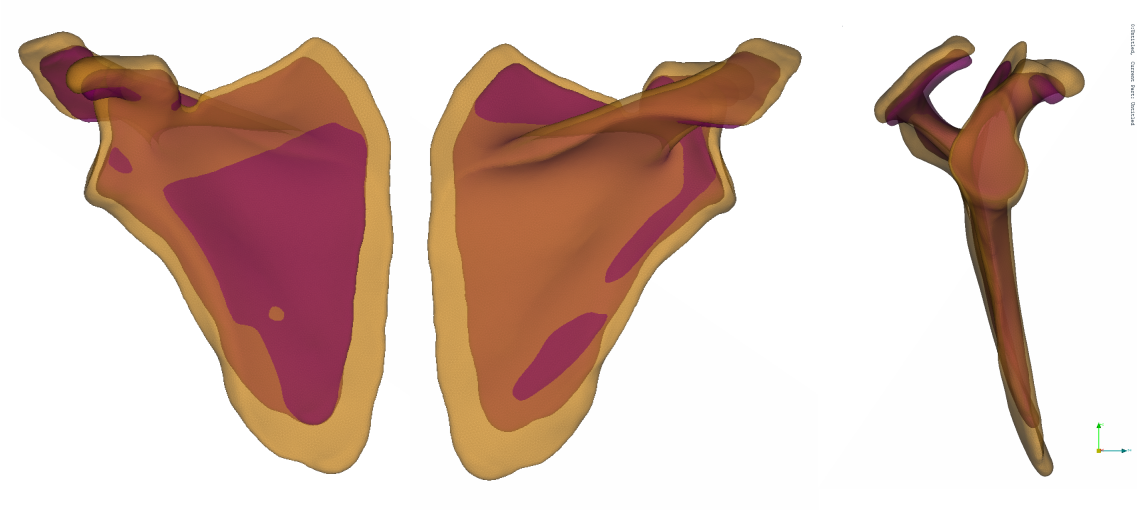

Figure 4.3: Anterior, posterior, and medial view of the meshes created by the PC scores with $\mu \pm \sigma$ on PC 1. Yellow corresponds with $\mu + \sigma$ and purple corresponds with $\mu - \sigma$.

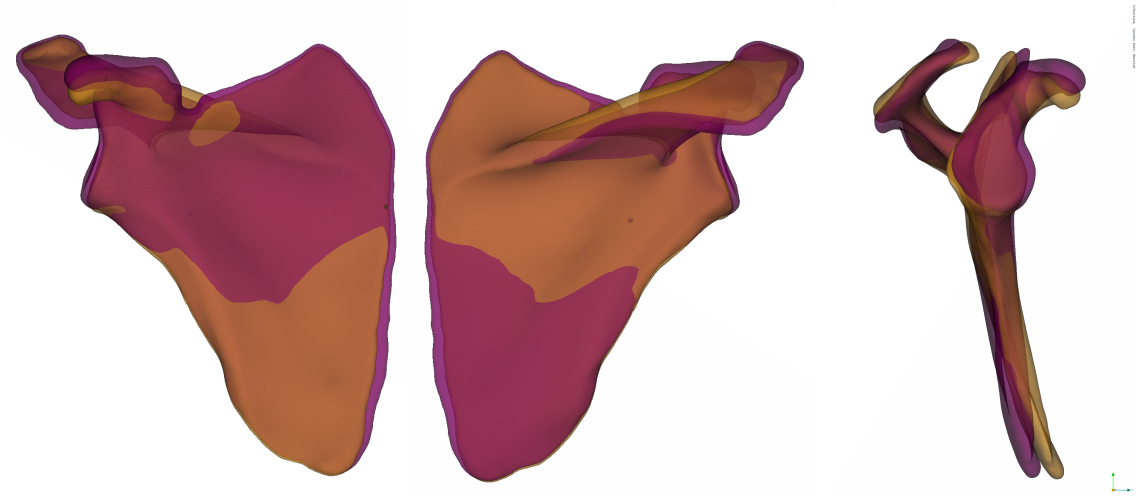

Figure 4.4: Anterior, posterior, and medial view of the meshes created by the PC scores with $\mu \pm \sigma$ on PC 2. Yellow corresponds with $\mu + \sigma$ and purple corresponds with $\mu - \sigma$.

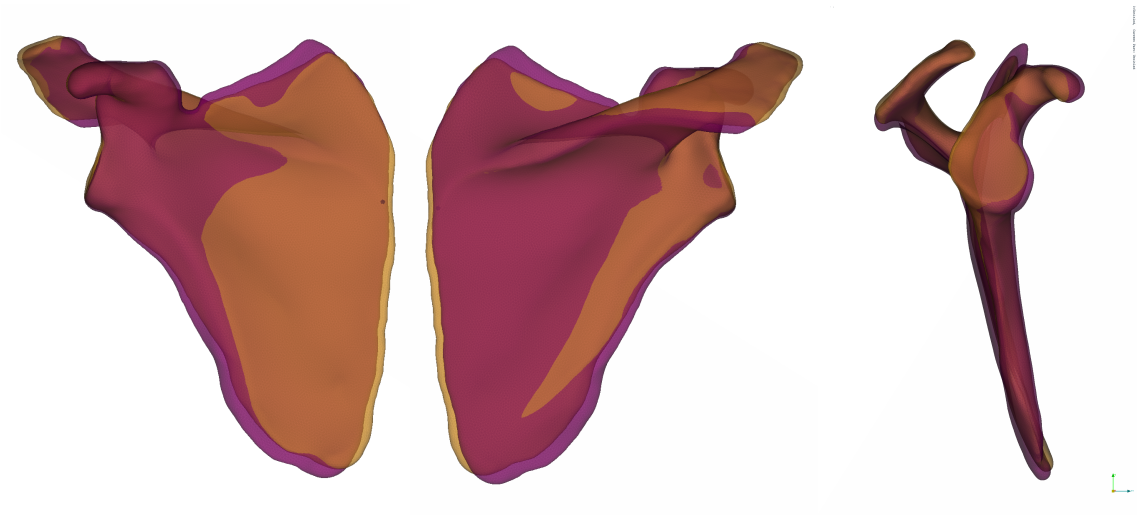

Figure 4.5: Anterior, posterior, and medial view of the meshes created by the PC scores with $\mu \pm \sigma$ on PC 3. Yellow corresponds with $\mu + \sigma$ and purple corresponds with $\mu - \sigma$.

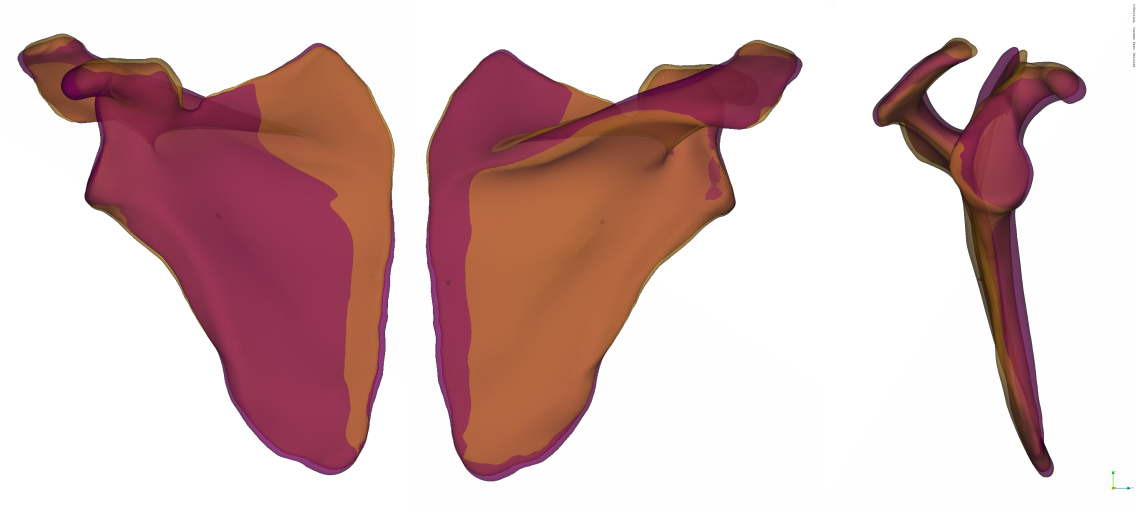

Figure 4.6: Anterior, posterior, and medial view of the meshes created by the PC scores with $\mu \pm \sigma$ on PC 4. Yellow corresponds with $\mu + \sigma$ and purple corresponds with $\mu - \sigma$.

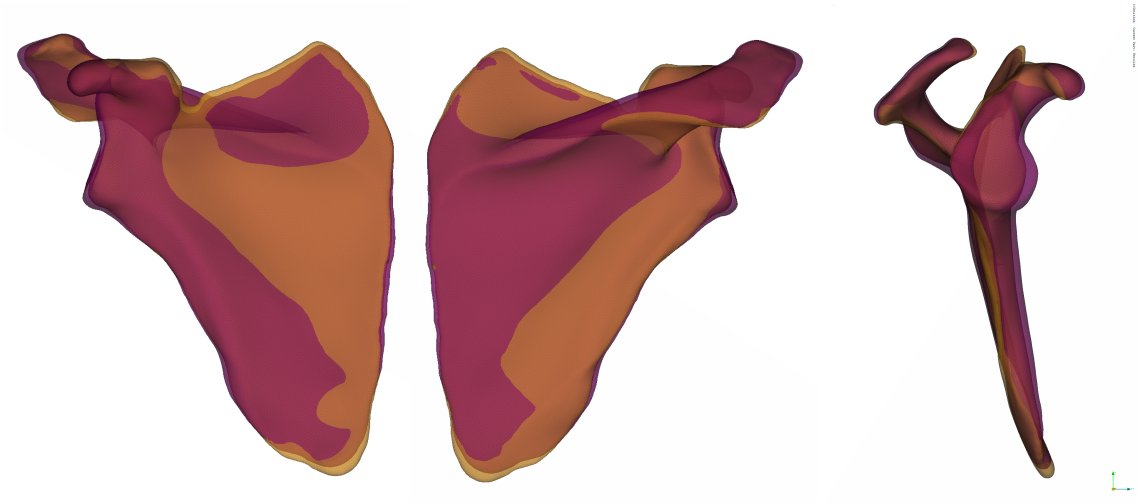

Figure 4.7: Anterior, posterior, and medial view of the meshes created by the PC scores with $\mu \pm \sigma$ on PC 5. Yellow corresponds with $\mu + \sigma$ and purple corresponds with $\mu - \sigma$.

4.4 Regression model

The used principal components and variables are displayed in Table 4.1. Out of the 16 components that were considered for the regression model, only $1, 5, 9, 10$, and 16 had significant variables ($p \leq 0.05$). The variables that never resulted in significance were BMI and sex*height.

Principal component	R^2	Significant variables ($p \leq 0.05$)
1	0.605	Height, Sex
2	-	
3	-	
4	-	
5	0.154	Healthy, Height
6	-	
7	-	
8	-	
9	-	
10	0.065	Sex
11	0.077	Age, Healthy
12	-	
13	-	
14	-	
15	-	
16	0.085	Age

Table 4.1: R^2-score and significant variables for the 16 principal components from the regression model. Components without significance are marked with "-" in R^2.

In Figure 4.8 minor differences can be seen in many places, including the acromion, coracoid process, and along the border, where the rhomboid minor is connected.

In Figure 4.9 the largest difference in scale can be seen around the inferior angle and up along the border towards the superior angle. No curvature or other differences can be spotted besides pure scale.

In Figure 4.10, PC5 has a significant effect on the healthy variable. A noticeable difference at the glenoid cavity can be seen, as well as further down towards the inferior angle, at the connection for the triceps brachii.

In Figure 4.11, a difference in size can be seen in most places, in particular along the rhomboid major between the superior and inferior angles. The curvature of both the scapular spine and the acromion differs, as well as the position of the coracoid process.

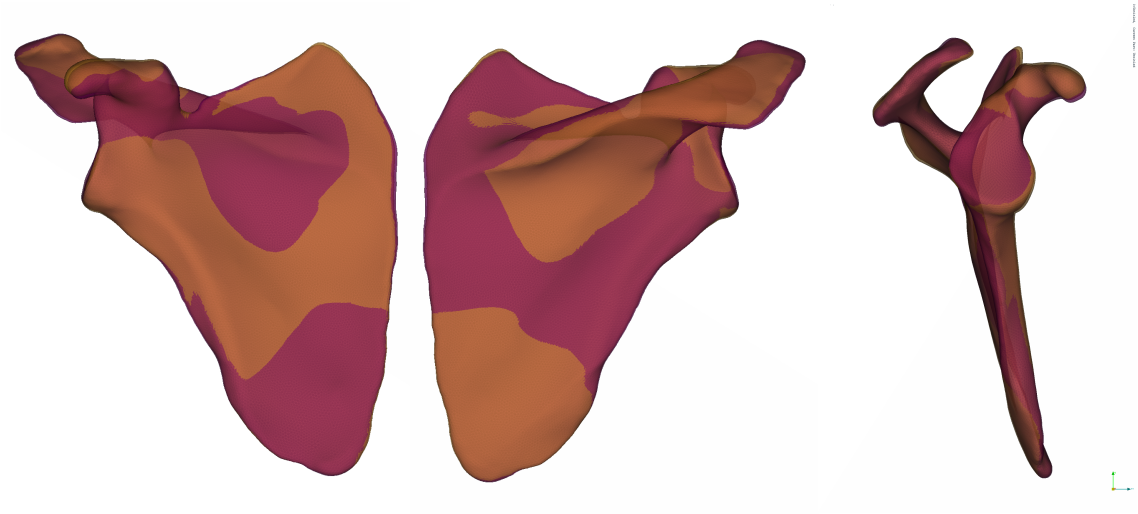

Figure 4.8: Anterior, posterior, and medial view of the meshes created by the prediction model with age 44.6 ± 18.9. Yellow corresponds with 63.5 years old, and purple corresponds with 25.7 years old.

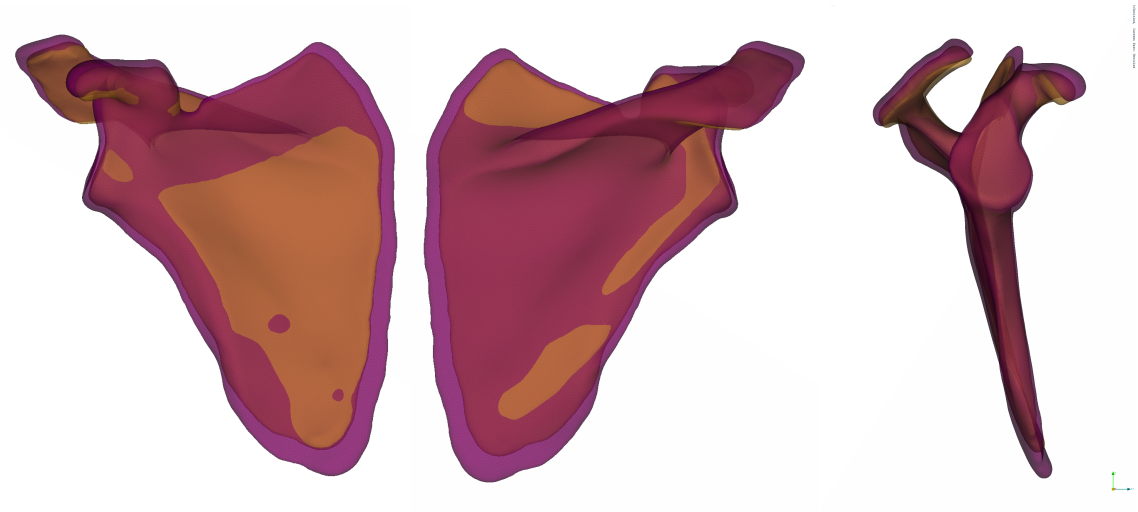

Figure 4.9: Anterior, posterior, and medial view of the meshes created by the prediction model with $1.74 \pm 0.11(m)$ for height. Purple corresponding with $1.85(m)$ and yellow corresponding with $1.63(m)$.

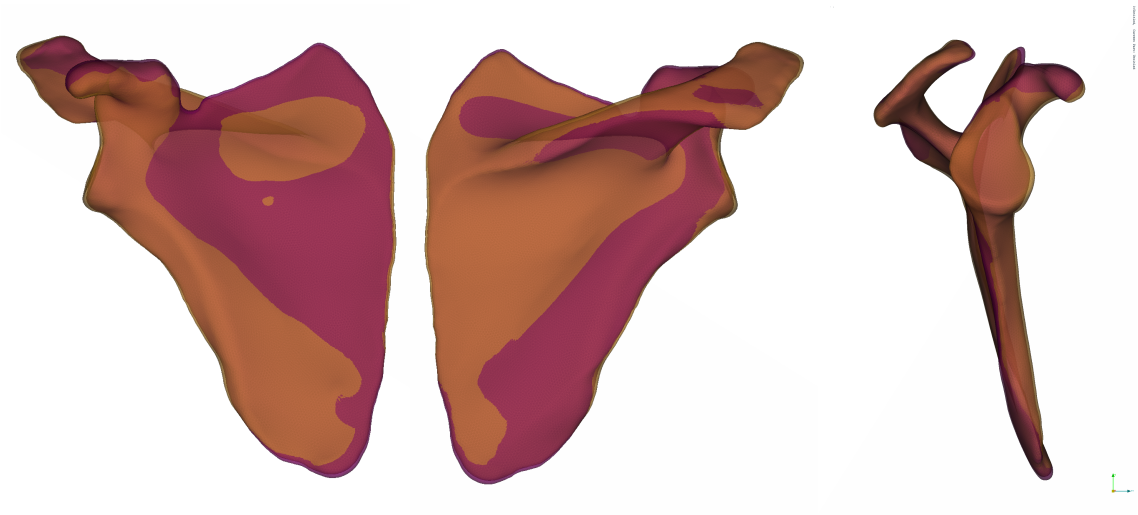

Figure 4.10: Anterior, posterior, and medial view of the meshes created by the prediction model on the "healthy" variable. Yellow corresponds with healthy, and purple corresponds with injured.

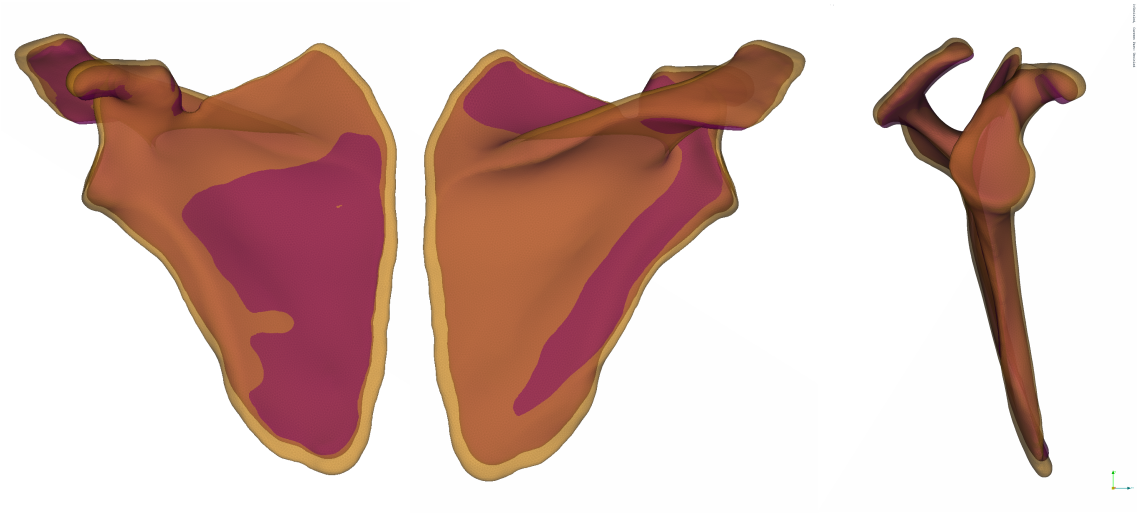

Figure 4.11: Anterior, posterior, and medial view of the meshes created by the prediction model for sex. Yellow corresponds with male, and purple corresponds with female.

5

Discussion

The project had several limitations; the workflow for creating the SSM is complex, and every step of the way is important for the finalized model. The design of the landmarks will affect both the resulting morph and the alignment of the GPA. The interpolation used in the morph and the algorithm used in the GPA will also give different results. With further attention to detail on the design of the landmarks and with an extensive comparison between different algorithms throughout the pipeline, further improvements can be made.

Designing a landmark schema is a process that relies on trial and error, something that could be infinitely improved until the entire surface is covered in landmarks. At some point, you have to decide that the resulting morphs are good enough and that the general shape of the bone is covered, even if minor details are missed. While the morphing resulting from this design of landmarks was, in general, quite good, there can always be improvements. Around the spine of the acromion, we have a denser distribution of landmarks, and down towards the inferior angle, we have a lot less, something which could impact the alignment for the GPA. With the denser top, the alignment might be biased towards alignment on the acromion and coracoid process instead of matching up the borders of the scapula. The higher density of landmarks on the top was made from the understanding that a majority of the injuries was related to the glenoid cavity and that higher detail would be beneficial at that location.

Even though the landmarks used in this study were selected with care, it should be noted that even a well-selected landmark schema can miss subtle details of scapular morphology. For example, how the ridges in the infraspinous fossa are orientated varies widely between samples and would require tens, if not a hundred landmarks on merely the fossa to capture precisely. This is a limitation inherent in the method and can affect the overall fidelity of the SSM since certain details of the anatomy are underrepresented or not represented at all. Furthermore, the generalizability of the model is inherently restricted by the demographic variables included in the study—i.e., sex, height, age, and BMI. As a result, the model may fail to represent morphological variation due to other demographic or lifestyle factors, e.g., ethnicity, medical condition, or physical activity level. It is conceivable that the inclusion of these factors in future studies could further enhance the validity and applicability of scapular statistical shape models.

The placement of the landmarks did not include a landmark on the infraspinous fossa or the subscapular fossa. The reason we did not include this landmark was

that the fossa was irregular enough that we could not place an anatomical landmark consistently. An alternative would be to place a semi-landmark on some set distance instead, which could provide additional information on the thickness of the fossa.

Another possible issue with the project is a lack of objective measurement and validation of the model, due to time constraints a cross-validation method could not be implemented. Instead we opted for using the R^2 of the components in comparison with similar models as well as comparing the length of predicted scapula percentiles to our actual data with similar demo-graphical data. A cross-validation method comparison to literature would be a

The used dataset is a combination of three smaller datasets, with one of the three sets containing Hill-Sachs injuries. The other two subsets was skewing towards older samples, with a high concentration in the ranges 50-70 years old. The portion of the data with a Hill-Sachs injury was included for a more uniform age distribution. The demographics of the data used in the model are presented in section 3.2 and Figure: 3.2a show a skewness in sex towards males. In addition, Figure: 3.2c shows a higher concentration in 20-30 years old and 55-70 year old and there is the possibility that the model is missing information in the 30-55 age range. The Figures: 3.2d and 3.2b show the BMI and height distribution which are normally distributed and cover a large range of the values.

One unintended consequence of this choice of dataset was that one of the three portions of the set was scapulae with Hill-Sachs lesions. The scapulae with lesions were included because the demographics of said dataset were younger in years and therefore gave us better coverage from the data. The initial remedy for this Hill-Sachs lesion was to simply landmark as close as possible to where the landmark would be in the case of no lesion. In some cases, there is no mesh where you want to put the landmark since the lesion resulted in a scraping of or dislodging of bone tissue. A parameter to control for this injury was included, and gave us a statistical significant result for one of the principal components. With this parameter in place, we were able to see a slight change in the resulting meshes made for healthy or injured scapulae. What started as a problem with the dataset gave us a possible insight into how a Hill-Sachs injury changes the glenoid cavity.

For future work, an interesting comparison could be made for the density of the landmarks. How would the GPA behave for different densities of landmarks. Would a more uniform distribution of landmarks give a better alignment for the rotational matrix or how much of an impact does this have on the final model.

6
Conclusion

The primary objective of this project was to develop a statistical shape model for the human scapula, and this objective has been successfully achieved. The resulting model demonstrates a realistic prediction of size and shape, incorporating in lesser detail additional features such as curvature and thickness of bone sections.

In summary, this research contributes to the understanding of scapular morphology and, in part, the implications of injuries such as Hill-Sachs lesions. However, limitations exist, particularly regarding the dataset and methodology. Future work should focus on refining landmark design and exploring the effects of landmark distribution on model performance. This model lays the groundwork for further exploration in the field of statistical shape modeling of the scapula and its applications in injury prevention.

Bibliography

[1] F. Zhao et al. *Current Progress of Digital Twin Construction Using Medical Imaging*. arXiv. 2024. URL: https://arxiv.org/abs/2411.08173. Accessed: 2 Jun 2025.

[2] Matthew A. Varacallo. Paul T. Cowan Andrew Mudreac. *Anatomy, Back, Scapula*. Treasure Island (FL): StatPearls Publishing, 8-08-2023. URL: https://www.ncbi.nlm.nih.gov/books/NBK531475/. Accessed: 2 Jun 2025.

[3] Jānis Šavlovskis & Kristaps Raits. *Anatomy Standard*. 6-2020. URL: https://www.anatomystandard.com/ossa-et-juncturae/extremitas-superior/scapula.html. Accessed: 2 Jun 2025.

[4] . *Scapula - three views*. URL: https://commons.wikimedia.org/wiki/File:Scapula3views-star.jpg. Licensed under CC BY-SA 4.0, Accessed: 12 Jun 2025.

[5] Schmidt. Viktor et al. *Epidemiology, treatment, and mortality of 3973 scapula fractures from the Swedish fracture register*. 28-04-2024. URL: https://pubmed.ncbi.nlm.nih.gov/38688421/. Accessed: 2 Jun 2025.

[6] Larsson S. Ideberg R Grevsten S. *Incidence and classification of 338 fractures*. 9-1995. URL: https://pubmed.ncbi.nlm.nih.gov/7484114/. Accessed: 2 Jun 2025.

[7] Rolf Ideberg, Sven Grevsten, and Sune Larsson. *Epidemiology of scapular fractures incidence and classification of 338 fractures*. 1995. URL: https://www.tandfonline.com/doi/abs/10.3109/17453679508995571. Accessed: 2 Jun 2025.

[8] Michal TUčEK et al. *Epidemiology of scapular fractures*. 2017. URL: https://www.actaorthopaedica.be/assets/2479/02-Tucek-.pdf?utm_medium=email&utm_source=transaction. Accessed: 2 Jun 2025.

[9] National Institute of Arthritis, Musculoskeletal, and Skin Diseases (NIAMS). *Osteoporosis*. n.d. URL: https://www.niams.nih.gov/health-topics/osteoporosis. Accessed: February 5, 2025.

[10] Matthew T. Provencher et al. "The Hill-Sachs lesion: diagnosis, classification, and management". In: *Journal of the American Academy of Orthopaedic Surgeons* 20.4 (2012), pp. 242–252. URL: https://journals.lww.com/jaaos/fulltext/2012/04000/the_hill_sachs_lesion__diagnosis,_classification,.5.aspx. Accessed: 2 Jun 2025.

[11] Shoulder Doc. *Hill-Sachs Lesion*. Dec. 2023. URL: https://www.shoulderdoc.co.uk/article/1470. Accessed: 2 Jun 2025.

[12] Radiopaedia. *Hill-Sachs defect*. Dec. 2023. URL: https://radiopaedia.org/articles/hill-sachs-defect?lang=gb. Accessed: 2 Jun 2025.

[13] F. Ambellan et al. *Statistical Shape Models: Understanding and Mastering Variation in Anatomy*. Adv Exp Med Biol. 2019;1156:67-84. PMID: 31338778. 2019. DOI: 10.1007/978-3-030-19385-0_5. URL: https://pubmed.ncbi.nlm.nih.gov/31338778/. Accessed: 2 Jun 2025.

[14] Johan Iraeus. *Quantifying human skeletal variability - from medical images using state-of-the-art methods*. URL: https://annonsportal.chalmers.se/CareerServices/en/Ads/Details/2803. Accessed: 2 Jun 2025.

[15] Giovanni Belingardi Filippo Germanetti Dario Fiumarella and Alessandro Scattina. *Injury Criteria for Vehicle Safety Assessment: A Review with a Focus Using Human Body Models*. 9 August 2022. URL: https://doi.org/10.3390/vehicles4040057. Accessed: Accessed: 2 Jun 2025.

[16] Oscar Hallberg Chiara Fichera. *Presentation: From CT Scans to Statistical Shape Models*. 25-01-21.

[17] T. Heimann and H. P. Meinzer. *Statistical shape models for 3D medical image segmentation: A review*. Medical Image Analysis. 2009. URL: https://doi.org/10.1016/j.media.2009.05.004. Accessed: 17 Jun 2025.

[18] Christoph Witzgall Jim Lawrence Javier Bernal. *A Purely Algebraic Justification of the Kabsch-Umeyama Algorithm*. Oct. 2019. URL: https://nvlpubs.nist.gov/nistpubs/jres/124/jres.124.028.pdf. Accessed: 3 Jun 2025.

[19] Mark H. Holmes. *Introduction to Scientific Computing and Data Analysis. Texts in Computational Science and Engineering (2nd ed.). Springer. pp. 475–490.* 2023.

[20] AV. *Derivation of the Least Squares Estimator for Beta in Matrix Notation*. 2015. URL: https://economictheoryblog.com/2015/02/19/ols_estimator/. Accessed: 17 Jun 2025.

[21] Heath B Henninger. *3D models of the human scapula and humerus with defined anatomic landmarks*. 2-01-2025. URL: https://zenodo.org/records/14590062. Accessed: 2 Jun 2025.

[22] URL: https://github.com/infekit/infepy. Accessed: 17 Jun 2025.

A

Appendix 1

Descriptions of the anatomical landmarks used for placement on the scapula:

Landmark	Description
1	The landmark is placed at the center of the glenoid fossa. Landmarks 1–5 together form a cross over the glenoid cavity.
2	This landmark is located at the bottom of the glenoid cavity, positioned towards the inferior angle of the scapula.
3	The landmark is positioned on the side of the glenoid cavity closest to the coracoid process.
4	The landmark is placed on the side of the glenoid cavity closest to the acromion.
5	This landmark is positioned at the top of the glenoid cavity, directed towards the superior angle.
6	The landmark is located at the deepest part of the space between the glenoid cavity and the coracoid process, centered in the middle of the coracoid process.
7	This landmark is at the top of the scapular notch, positioned towards the coracoid process. Landmarks 7–10 estimate the boundaries of the coracoid process.
8	The landmark is placed on the edge of the coracoid process.
9	This landmark is located on the side of the coracoid process closest to the glenoid cavity, in front of the acromion.
10	The landmark is found on the opposite side of the coracoid process, on the anterior surface of the scapula.
11	The landmark is positioned at the bottom of the scapular notch.
12	The landmark is located at the top of the scapular notch, directed towards the superior border.
13	This landmark is placed at the top of the superior border, also known as the superior angle.
14	The landmark is found on the medial border of the scapula, where the spine of the scapula is centered.
15	The landmark is on the left side of the acromion extremity, facing the scapular notch. Landmarks 15–17 form a triangle on the acromion.
16	The landmark is located on the right side of the acromion extremity, oriented towards the glenoid cavity.
17	This landmark is at the bottom of the acromion extremity, facing the inferior angle.

18	The landmark is placed at the deepest part of the connection between the glenoid cavity and the acromion, located on the glenoid cavity.
19	The landmark is found at the furthest point of the inferior angle.
20	This landmark is the midpoint along the edge between landmarks 16 and 17.
21	The landmark is located at the midpoint of the distance between landmarks 15 and 20, on the top of the acromion.
22	This landmark is positioned at the center of the first sixth of the distance between landmarks 21 and 14 along the scapular spine. Landmarks 22–26 divide this segment into six equal parts.
23	The landmark is at the center of the second sixth between landmarks 21 and 14.
24	The landmark is at the center of the third sixth between landmarks 21 and 14.
25	The landmark is at the center of the fourth sixth between landmarks 21 and 14.
26	The landmark is at the center of the fifth sixth between landmarks 21 and 14.
27	The landmark is placed on the curvature of the scapular spine, on the right side of landmark 22, following the direction of landmark 15 and opposite landmark 17.
28	The landmark is on the side of landmark 23 closest to landmark 17, at the corner of the scapular spine.
29	The landmark is on the side of landmark 23 closest to landmark 27, at the corner of the scapular spine.
30	The landmark is on the side of landmark 24 closest to landmark 17, at the corner of the scapular spine.
31	The landmark is on the side of landmark 24 closest to landmark 27, at the corner of the scapular spine.
32	The landmark is on the side of landmark 25 closest to landmark 17, at the corner of the scapular spine.
33	The landmark is on the side of landmark 25 closest to landmark 27, at the corner of the scapular spine.
34	The landmark is on the side of landmark 26 closest to landmark 17, at the corner of the scapular spine.
35	The landmark is on the side of landmark 26 closest to landmark 27, at the corner of the scapular spine.
36	The landmark is located at the deepest part inside the spine of the acromion.
37	This landmark is at the midpoint between landmarks 13 and 12 along the superior border.
38	The landmark is positioned at one-quarter of the initial segment between landmarks 2 and 19 on the lateral (axillary) border.
39	The landmark is positioned at one-quarter of the secondary segment between landmarks 2 and 19 on the lateral (axillary) border.
40	The landmark is positioned at one-quarter of the third segment between landmarks 2 and 19 on the lateral (axillary) border.

41	The landmark is located at one-third of the initial segment between landmarks 19 and 14 on the medial (vertebral) border.
42	The landmark is located at one-third of the secondary segment between landmarks 19 and 14 on the medial (vertebral) border.
43	This landmark is at the midpoint between landmarks 13 and 14 on the medial (vertebral) border.
44	The landmark is at the midpoint between landmarks 20 and 15, on the underside of the acromion. The position is adjusted to create a smooth line between these two points.
45	This landmark is at the midpoint between landmarks 44 and 36, on the underside of the acromion.

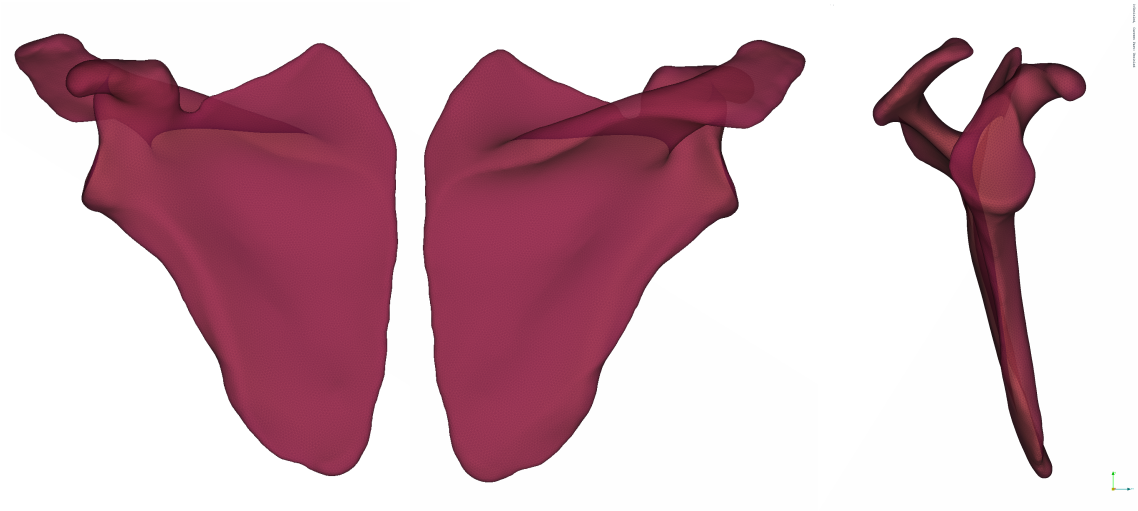

Figure A.1: Anterior, posterior, and medial view of the meshes created by the prediction model with $25.6 \pm 5.11 \frac{kg}{m^2}$ for BMI. Yellow corresponding with $30.71 \frac{kg}{m^2}$ and purple corresponding with $20.49 \frac{kg}{m^2}$. BMI does not have any impact on any anatomical feature.

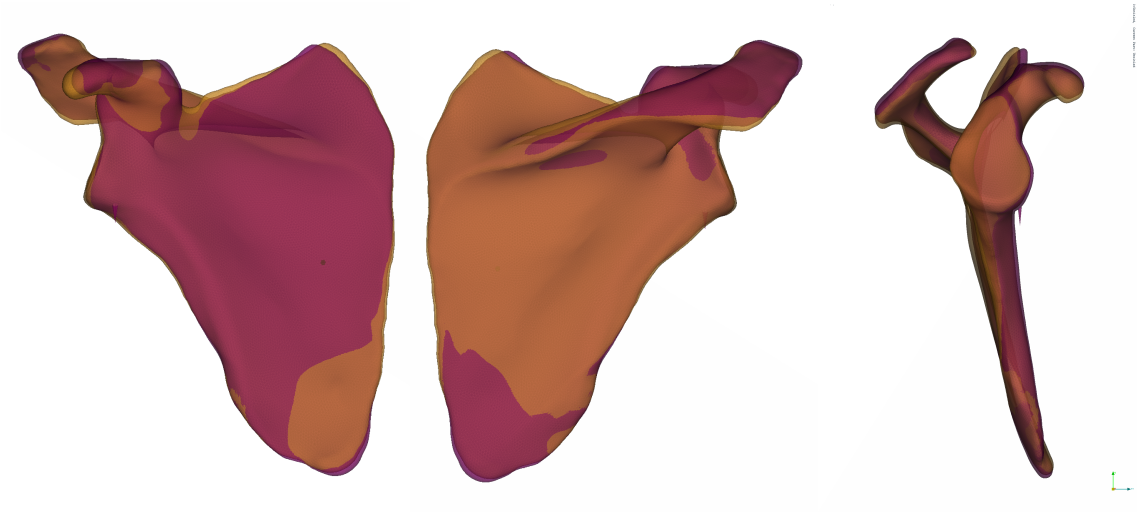

Figure A.2: Anterior, posterior, and medial view of the meshes created by the PC scores with $\mu \pm \sigma$ on PC 10. Yellow corresponds with $\mu + \sigma$ and purple corresponds with $\mu - \sigma$. Change in length of the coracoid process. Minor differences in the curvature for the superior angle and coracoid process. The suprascapular notch is moved vertically.

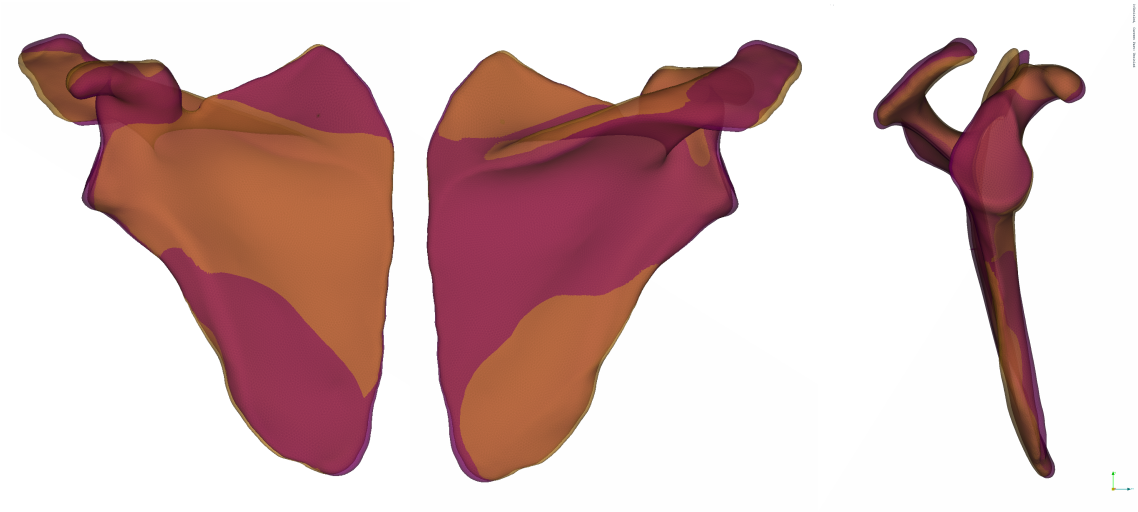

Figure A.3: Anterior, posterior, and medial view of the meshes created by the PC scores with $\mu \pm \sigma$ on PC 11. Yellow corresponds with $\mu + \sigma$ and purple corresponds with $\mu - \sigma$. A minor difference can be spotted at the superior angle.

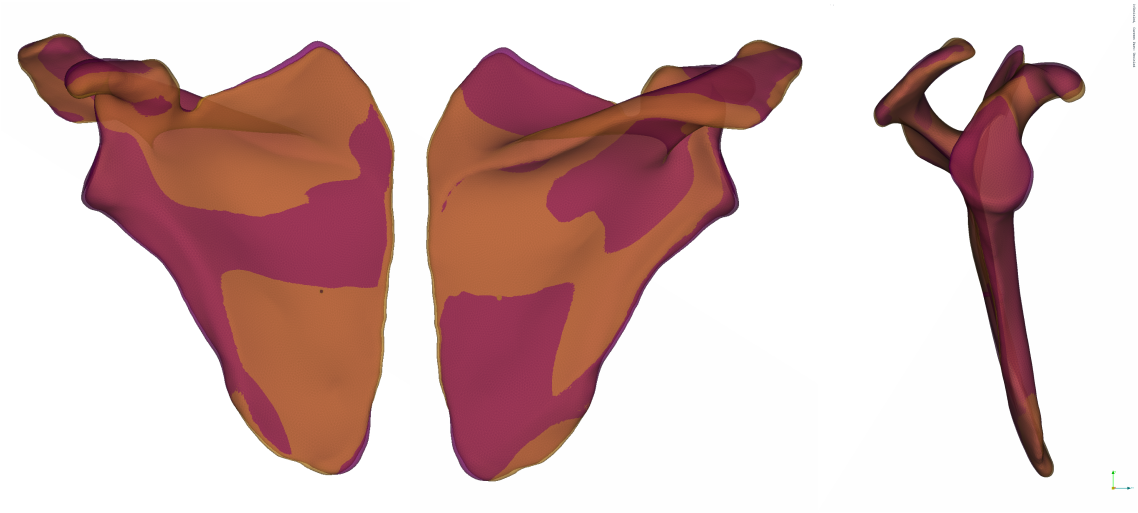

Figure A.4: Anterior, posterior, and medial view of the meshes created by the PC scores with $\mu \pm \sigma$ on PC 16. Yellow corresponds with $\mu + \sigma$ and purple corresponds with $\mu - \sigma$. Very minor differences can be spotted at the coracoid process and the entire border around the scapula.

DEPARTMENT OF MECHANICS AND MARITIME SCIENCES
CHALMERS UNIVERSITY OF TECHNOLOGY
Gothenburg, Sweden
www.chalmers.se

CHALMERS
UNIVERSITY OF TECHNOLOGY